Contribution of Rossby wave component to the equatorial wave structure of the Madden-Julian Oscillation

Jialin Lin[1,2], Minghua Zhang[1] and Brian Mapes[2]

[1] **State University of New York, Stony Brook, NY 11794**
[2] **NOAA-CIRES Climate Diagnostics Center, Boulder, CO 80305**

August, 2002

ABSTRACT

A Kelvin-wave conceptual model has often been used in studying wave-convection feedbacks in the Madden-Julian Oscillation (MJO). This study examines whether the equatorial wave structure of the MJO is similar to a pure Kelvin wave, using long term observations from tropical sounding stations and NCEP reanalysis, supplemented by measurements from the Tropical Ocean Global Atmosphere (TOGA) Coupled Ocean Atmosphere Response Experiment. All datasets are filtered using a 30-70 day bandpass filter. The long-term MJO composites are constructed using linear correlation and linear regression with respect to precipitation.

The observed equatorial wave structure of the MJO is different from the Kelvin wave, in that the geopotential height lags the zonal wind by a quarter cycle, which is different from the in-phase relationship in the Kelvin wave.

The horizontal wave structure of the MJO is similar to the Matsuno-Gill pattern with a strong Rossby wave component. Based on the Gill model, the strong Rossby wave component significantly shifts the *equatorial* geopotential height anomaly westward, and makes the equatorial wave structure different from the Kelvin wave.

It is shown that the wave-convection feedback mechanisms in the observed Kelvin-Rossby wave are different from those in the Kelvin wave model. This is because the Rossby wave component significantly shifts the equatorial temperature anomaly westward, and changes its phase relations with the heating terms associated with the free troposphere moisture convergence, the boundary layer moisture convergence, the surface heat flux, and the local drying of moisture. Therefore, the Rossby wave

component needs to be taken into account when studying wave-convection feedbacks in the MJO.

1. Introduction

Discovered by Madden and Julian (1971, 1972), the Madden-Julian Oscillation (MJO) is the dominant intraseasonal mode in tropical convection and circulation (e.g. Weickmann et al. 1985, Lau and Chan 1985, Salby and Hendon 1994, Wheeler and Kiladis 1998). It affects a wide range of tropical weather such as the onset and breaks of the Indian and Australian summer monsoons (e.g. Yasunari 1979, Hendon and Liebmann 1990), and the formation of tropical cyclones (e.g. Nakazawa 1986, Liebmann et al. 1994). It also drives teleconnections to the extratropics (e.g., Lau and Phillips 1986) and impacts some important extratropical weather. On a longer timescale, the MJO is observed to trigger or terminate some El Nino events (e.g. Kessler et al. 1995, Takayabu et al. 1999, Bergman et al. 2001). Therefore, the MJO is important for both extended-range weather forecasting and long-term climate prediction.

A Kelvin-wave conceptual model has often been used in studying the wave-convection feedback mechanisms in the MJO, such as the wave-CISK (Convective Instability of the Second Kind) mechanism (e.g. Takahashi 1987, Chang and Lim 1988, Lim et al. 1990, Crum and Dunkerton 1992), the frictional wave-CISK mechanism (e.g. Wang 1988, Moskowitz and Bretherton 2000), the WISHE (Wave Induced Surface Heat Exchange) mechanism (e.g. Emanuel 1987, Neelin et al. 1987, Crum and Dunkerton 1994), the phase-lagged wave-CISK mechanism (e.g. Cho et al. 1994), and the phase-lagged WISHE mechanism (e.g. Emanual 1993, Neelin and Yu 1994, Yu and Neelin 1994, Goswami and Rao 1994). The usage of a Kelvin-wave model was justified by the

following characteristics of the MJO from the early observations (Madden and Julian 1971, 1972, Parker 1973): (1) the eastward propagation, (2) the absence of large amplitude in the meridional wind component near the equator, (3) the absence of Rossby gyres at low levels. Later observational studies (e.g. Weickmann et al. 1985, Knutson and Weickmann 1987, Rui and Wang 1990, Salby and Hendon 1994) showed that the upper level wind structure of the MJO has Rossby gyres in the subtropics, but the wind structure along the equator still shows the first two characteristics, which are similar to the Kelvin wave.

However, another characteristic of the Kelvin wave, which is important for wave-convection feedback, is the in-phase relationship between zonal wind and geopotential height. Only a few observational studies analysed the phase relation between zonal wind and geopotential height (or temperature) in the MJO (Hendon and Salby 1994, Kiladis and Weickmann 1992, Hsu 1996), and they showed inconsistent results.

Hendon and Salby (1994) constructed the composite life cycle of the MJO using temperature from the MSU channel 2 and wind from a four-dimensional assimilation product. They found that as the MJO moves eastward from the western Indian Ocean to the central Pacific Ocean, the MSU channel 2 temperature is always nearly in phase with the 200 mb zonal wind. Assuming that the geopotential height has a simple baroclinic structure along the equator and the MSU channel 2 temperature represents the troposphere mean temperature, the 200 mb geopotential height would also be in phase with the 200 mb zonal wind. This is similar to the Kelvin wave.

On the contrary, Kiladis and Weickmann (1992) and Hsu (1996) constructed the

composite life cycle of the MJO using wind and geopotential height data both from the four-dimensional assimilation. They found that over the western Pacific Ocean, the 200 mb geopotential height lags the zonal wind by a quarter cycle. This is different from the Kelvin wave.

The motivation of this study is to use the in situ sounding data to check which of the above two results is correct. Madden and Julian (1971, 1972, 1994) and Nishi (1989) used the sounding data to calculate the phase difference between the zonal wind and the geopotential height. As reviewed by Madden and Julian (1994), the results are complex. Their method is somehow different from the above three papers (Hendon and Salby 1994, Kiladis and Weickmann 1992, Hsu 1996) which used deep convection as the reference time series. In order to compare with the results of Hendon and Salby (1994), Kiladis and Weickmann (1992), and Hsu (1996), in this study we use deep convection as the reference time series.

The datasets used in this study are described in section 2. Methods are described in section 3. Results are reported in section 4. Summary is given in section 5.

2. Data

The datasets used include long-term data and TOGA COARE data.

The long term datasets cover 21 years from 1979 to 1999. They include:

(1) The upper air sounding from the tropical stations (Fig. 1). The variables used include wind, geopotential height and temperature at 12 mandatory levels. We average the data at each station to pentad data. There are only a few missing data.

They are filled with linear interpolation.

(2) The daily NCEP reanalysis data. The variables used include upper air wind, geopotential height, temperature and specific humidity, and surface latent and sensible heat fluxes. The horizontal resolution is 2.5 degree longitude by 2.5 degree latitude. We average the data along the equator (between 5N and 5S) to pentad data with a zonal resolution of 10 degree longitude.

(3) The pentad NCEP Chi-corrected divergence and vertical motion profiles calculated by Sardeshmukh et al. (1999). The horizontal resolution is 2.5 degree longitude by 2.5 degree latitude. We average the data along the equator (between 5N and 5S) with a zonal resolution of 10 degree longitude. This data is dynamically consistent diabatic heating derived from twice-daily NCEP reanalyses. See Sardesmukh et al. (1999) for details of the technique.

(4) The pentad CMAP precipitation calculated by Xie and Arkin (1997). The horizontal resolution is 2.5 degree longitude by 2.5 degree latitude. We average the data along the equator (between 5N and 5S) with a zonal resolution of 5 degree longitude.

The TOGA COARE datasets cover 120 day from November 1, 1992 to Feburary 28, 1993. They include:

(1) the 6-hourly IFA sounding array budgets calculated by Ciesilski et al. (2002),

(2) the daily OSA sounding array budgets calculated by us using the method of Zhang and Lin (1997), and

(3) the 3-hourly IFA surface precipitation, latent heat flux and sensible heat flux calculated by Curry et al. (2001).

3. Method

All datasets are filtered using a 30-70 day Murakami (1976) filter, whose response function is shown in Fig. 2. The central frequency correspond to a period of 45 day. The half amplitude is at periods of 30 day and 70 day.

For the TOGA COARE data, there are two MJO events (see e.g. Chen et al 1996). We focus on the December 1992 event which is stronger and has better data availability. The maximum of the 30-70 day bandpass filtered precipitation anomaly at the location of the COARE measurements is at December 19, 1992.

For the long term data, an MJO composite is constructed using linear regression with respect to an MJO index. In this study, we use filtered CMAP precipitation as our MJO index. Because the MJO is a large-scale phenomenon dominated by wavenumber 0-6 (Wheeler and Kiladis 1998), the CMAP precipitation has been zonally filtered to keep only wavenumber 0-6. The confidence level of linear correlation is estimated following Oort and Yienger (1996).

4. Results

4.1 Equatorial wave structure of the MJO

Fig. 3 shows the vertical structure of MJO at 0N155E from 21 years of NCEP reanalysis data. The time lag is with respect to the time of maximum precipitation. The time evolution is from the right to the left, showing the local evolution of heating as the eastward-moving MJO passes the measurement longitude. The zonal wind (Fig.

3a) shows a simple two-layer structure with the upper layer out of phase with the lower layer. This two-layer structure is well-known from many previous observations (e.g. Madden and Julian 1971, 1972, Weickmann et al. 1985, Knutzson and Weickmann 1987). An interesting feature which did not bring much attention is that the maxima of both the two layers are at a very high altitude, not the 850 mb and 200 mb levels generally used in MJO studies. The maximum of the lower layer is around 600 mb (just below the 0 C level), while that of the upper layer is around 150 mb (just below the tropopause). It means that at the time of maximum precipitation, the zonal inflow is just below the 0 C level, and the zonal outflow is just below the tropopause. Consistent with this inflow-outflow feature, the vertical motion (Fig. 3b) concentrates in the upper troposphere. For clarity, the two-dimensional flow is plotted using arrows in Fig. 3c. This middle troposphere inflow and near tropopause outflow structure are consistent with the top-heavy heating profile shown in Lin et al. (2002).

The vertical motion shows a westward phase tilt with height. It develops first in the lower troposphere, and then shifts upward as it intensifies. This westward phase tilt of vertical motion is consistent with the westward phase tilt of the associated heating anomaly shown in Lin et al. (2002), and may reflect or indicate more shallow convection in the earlier stage, and more stratiform precipitation in the later stage.

The geopotential height (contours in Fig. 3c) also shows a two-layer structure, with the upper layer out of phase with the lower layer. The node is also at high level around 350 mb, as high as that of the zonal wind.

Notice the phase difference between the geopotential height and the zonal wind,

which is a key indicator of the wave type. At the upper layer, the geopotential height lags the zonal wind by a quarter cycle. Because for both the zonal wind and the geopotential height the upper layer is out of phase with the lower layer, at the lower layer, the geopotential height also lags the zonal wind by a quarter cycle. This quarter cycle phase difference indicates that the equatorial wave structure of the MJO is not a Kelvin wave.

In summary, the equatorial wave structure of the MJO in the NCEP reanalysis has three characteristics: (1) The flow is middle-troposphere inflow and near tropopause outflow at the time of maximum precipitation. (2) The vertical motion has a westward phase tilt with height. (3) The zonal wind lags the geopotential height by a quarter cycle.

The quarter cycle phase difference is consistent with the results of Kiladis and Weickmann (1992) and Hsu (1996) using the operational analysis data, but inconsistent with the result of Hendon and Salby (1994) using the MSU channel 2 temperature data. Therefore next we use the in situ sounding data to validate the above results. Fig. 4 is the same as Fig. 3 except for the MJO event observed by TOGA COARE Outer Sounding Array (OSA). The zonal wind (Fig. 4a), vertical motion (Fig. 4b), and geopotential height (Fig. 4c) all look similar to the NCEP reanalysis composite in Fig. 3, showing the three characteristics listed above. An MJO composite of 21 years of sounding data at Pohnpei (Fig. 5) also supports the NCEP reanalysis composite, especially the quarter cycle phase difference between the zonal wind and the geopotential height. Further analysis of the sounding data from other stations

(Chuuk, Honiara) gives similar results (not shown). Therefore the in situ sounding data support the NCEP reanalysis composite and the results of Kiladis and Weickmann (1992) and Hsu (1996), but does not support the result of Hendon and Salby (1994).

Why does the MSU channel 2 temperature used by Hendon and Salby (1994) give different result? The answer lies in the vertical structure of the temperature anomaly in the MJO (Fig. 6). Consistent with the geopotential height anomaly (Fig. 3c, Fig. 4c, Fig. 5b), the temperature anomaly concentrates in the upper troposphere, and is nearly in phase with the precipitation and upward motion. The temperature anomaly in the lower troposphere is very small, and tends to lead that in the upper troposphere. The MSU channel 2 temperature used in Hendon and Salby (1994) has most of its weighting from the lower and middle troposphere (Spencer et al. 1990, their Fig. 1). Therefore, the MSU channel 2 is not suitable for representing the troposphere mean temperature in the MJO.

We do not have access to the MSU channel 2 temperature data, but we have obtained a new version of the MSU temperature which seperates the upper troposphere temperature (called MSU34) and the lower troposphere temperature (called MSU23). The weighting function of MSU channel 2 temperature is similar to that of MSU23. Fig. 7 shows the MJO composite of (a) MSU34 and (b) MSU23 at 0N155E. We can see that MSU34 nearly in phase with the precipitation, which is consistent with the upper troposphere temperature in the sounding data. MSU23 leads the precipitation by more than a quarter cycle, which is similar to the lower troposphere temperature

in the sounding data. Therefore, MSU34 is better in representing the upper troposphere temperature anomaly in the MJO.

4.2 Contribution of Rossby wave component to the equatorial wave structure

What makes the equatorial wave structure of the MJO differ from the Kelvin wave? To answer this question, we first look at the horizontal wave structure of the MJO. Fig. 8 shows the horizontal pattern of the geopotential height anomaly at (a) 150 mb and (b) 700 mb. For clarity, we plot the component symmetric to the equator. At the upper level (Fig. 8a), the Rossby component is very strong: for example, the amplitude of Z anomaly at 25 degree latitude is 12 m, while that along the equator is only 3 m.

The horizontal wave structure of the MJO resembles the Matsuno-Gill pattern (Matsuno 1966, Gill 1980). From the thermal forcing model of Gill (1980), Chao (1987) and Yamagata (1987), we know that a moving heating forces a coupled Kelvin-Rossby wave (Fig. 9a), which contains a Kelvin wave component (Fig. 9b) and a Rossby wave component (Fig. 9c). One thing which may not draw much attention is that the Rossby wave component can affect the *equatorial* wave structure, because the geopotential height of the Rossby wave component has a large amplitude at the equator (the right-hand curve in Fig. 9c). When the Rossby wave component is strong, it significantly shifts the equatorial Z anomaly westward, and makes the equatorial wave structure different from the case of a pure Kelvin wave.

4.3 Schematics of the observed MJO wave structure

Fig. 10 shows the schematics of the observed MJO wave structure. It has the following characteristics:

(1) At the time of maximum precipitation, the inflow is at the middle troposphere and the outflow is near the tropopause.

(2) The vertical motion has a westward phase tilt with height.

(3) The equatorial wave structure is different from the Kelvin wave, with the zonal wind lagging the geopotential height by a quarter cycle.

(4) The horizontal wave structure is similar to the Matsuno-Gill pattern with a strong Rossby wave component.

4.4 Effect of equatorial wave structure on wave-convection feedback

As discussed in the introduction, a Kelvin-wave conceptual model has often been used in studying wave-convection feedback in the MJO. The above results show that the observed equatorial wave structure is different from a pure Kelvin wave. How much does the difference affect the inferred wave-convection feedback processes?

Historically, different types of wave-convection feedback mechanisms emphasized different convective heating terms. With the aid of the column-integrated moisture budget and neglecting horizontal eddy fluxes, the column-integrated convective heat-

ing can be written as (Yanai and Johnson 1993):

$$\begin{aligned}\int_{p_t}^{p_s} Q_c dp &= LP + S \\ &= \int_{p_t}^{p_b} (-L \bigtriangledown \cdot \overline{q}\,\overline{\mathbf{v}})\, dp \; + \int_{p_b}^{p_s} (-L \bigtriangledown \cdot \overline{q}\,\overline{\mathbf{v}})\, dp \\ &\quad +(LE + S) \; + \int_{p_t}^{p_s} (-L \frac{\partial \overline{q}}{\partial t})\, dp \end{aligned} \tag{1}$$

where Q_c is the convective heating, p_t is the tropopause pressure, p_s the surface pressure, p_b the pressure at the top of the boundary layer, L the latent heat of vaporization, P is the surface precipitation, S the surface sensible heat flux, q the mixing ratio of water vapor, $\mathbf{v}$ the horizontal velocity, ω the vertical velocity, and E the surface evaporation rate. $\bigtriangledown$ is the isobaric del operator. The overbar denotes the running horizontal average. The first term in Eq. 1 is the free troposphere moisture convergence. The second term is the boundary layer moisture convergence. The third term is the surface heat flux. The last term is the column-integrated local drying of moisture. These four terms have been emphasized by the wave-CISK mechanism, the frictional wave-CISK mechanism, the WISHE mechanism, and the charge-discharge mechanism, respectively.

Fig. 11 shows these four heating terms during the life cycle of the MJO from three different datasets: TOGA COARE OSA (solid line), TOGA COARE IFA (dashed line), and 21 years of NCEP reanalysis (dash-dotted line). The free troposphere moisture convergence (Fig. 11a) is nearly in phase with the precipitation. The boundary layer troposphere moisture convergence (Fig. 11b) leads the precipitation by nearly a quarter cycle. The surface heat flux (Fig. 11c) lags the precipitation by about 0.1

cycle, which is consistent with previous observations (Jones and Weare 1996, Hendon and Glick 1997, Shinoda et al. 1998). The local drying of moisture (Fig. 11d) lags the precipitation by nearly a quarter cycle.

One key question for any given wave-convection feedback mechanism is the phase relationship between the heating term it emphasizes and the temperature anomaly. If they are in phase, the heating term tends to make the temperature anomaly amplify. If they are in quadrature, the heating term will contribute to horizontal propagation. As noted above, the observed equatorial wave structure has a different phase of the temperature anomaly than a pure Kelvin wave, in particular, the Rossby wave component shifts the temperature anomaly westward for a quarter cycle to be in phase with the vertical motion. This changes the phase relations between the temperature and the heating terms and therefore significantly affects the feedback mechanisms.

The wave-CISK mechanism (e.g. Hayashi 1970, Lindzen 1974, Lau and Peng 1987, Takahashi 1987, Chang and Lim 1988, Lim et al. 1990, Crum and Dunkerton 1992, Zhang and Geller 1994) emphasizes the free troposphere moisture convergence. In the Kelvin wave model, the free troposphere moisture convergence lags the temperature by nearly a quarter cycle (Fig. 12a). It could amplify the wave only when the wave has a westward tilt with height. In the observed Kelvin-Rossby wave, the Rossby wave component shifts the temperature anomaly westward to be in phase with the free troposphere moisture convergence (Fig. 13a). Therefore the free troposphere moisture convergence contributes an in-phase tendency to the equatorial temperature anomaly, without requiring a westward phase tilt of the wave.

The frictional wave-CISK mechanism (e.g. Hayashi 1971, Wang 1988, Rui and Wang 1990, Salby et al. 1994, Moskowitz and Bretherton 2000) emphasizes the boundary layer moisture convergence. In the Kelvin wave model, the boundary layer moisture convergence is nearly in phase with the temperature (Fig. 12b). In the observed Kelvin-Rossby wave, the boundary layer moisture convergence leads the temperature by less than a quarter cycle (Fig. 13b), contributing more of an eastward propagation tendency rather than amplification to the temperature anomaly.

The WISHE mechanism (e.g. Emanuel 1987, Neelin et al. 1987, Crum and Dunkerton 1994) emphysizes the surface latent and sensible heat flux. In the original WISHE theory, the mean surface wind is assumed to be easterly, which makes the anomalous surface wind speed, and therefore the surface heat flux in phase with the surface easterly (the dashed line in Fig. 12c). Then in the Kelvin wave model, the surface heat flux is in phase with the temperature anomaly and amplifies the wave. However, later observational studies (e.g. Zhang 1996, Lin and Johnson 1996, Jones and Weare 1996, Shinoda et al. 1998) show that the surface heat flux is nearly in phase with the surface westerly (the solid line in Fig. 12c). In the Kelvin wave model, this means that the surface heat flux is out of phase with the temperature anomaly and damps the wave, an apparent shortcoming of the WISHE mechanism for explaining the existance of the MJO. However, in the observed Kelvin-Rossby wave, the surface heat flux has positive correlation with the temperature anomaly (Fig. 13c), and therefore amplifies the wave.

The charge-discharge mechanism (Blade and Hartmann 1993) considered the local

variation of moisture in addition to the column-integrated moisture convergence and the surface heat flux. They proposed that the convective heating exists only when the upper air relative humidity is above a certain threshold value. The relative humidity threshold for deep convection makes the upper air moisture nearly in phase with the large-scale forcing. This mechanism has been investigated by many authors (e.g. Hayashi and Sumi 1986, Hayashi and Golder 1986, 1997, Lau et al. 1988, Itoh 1989, Raymond and Torres 1998, Wang and Shleshinger 1999), and is also called the "saturation triggering" by Hayashi and Golder (1997), and "preconditioning" by Raymond and Torres (1998). In this paper we will call it "charge-discharge" following Blade and Hartmann (1993) because this name emphasizes both the moistening before the deep convection and the drying after it. The phase-lagged wave-CISK mechanism (Hayashi 1971b, Kuo 1975, Cho et al. 1994), and the phase-lagged WISHE mechanism (Emanuel 1993, Neelin and Yu 1994, Goswami and Rao 1994) prescribe a difference between the large-scale forcing (the sum of the column-integrated moisture convergence and the surface heat flux) and the convective heating. This is equavalent to adding a third heating term whose phase is similar to that of the local drying of moisture.

In the Kelvin wave model, the local drying of moisture is nearly out of phase with the temperature and damps the wave (Fig. 12d). In the observed Kelvin-Rossby wave, the local drying of moisture lags the temperature by a quarter cycle (Fig. 13c) and therefore neither amplifies nor damps the temperature anomaly.

In summary, the westward phase shift of the temperature anomaly in the observed

Kelvin-Rossby wave relative to the theoretical Kelvin wave significantly affects the wave-convection feedback mechanisms. In the WISHE case, even the sign of the feedback is reversed. Therefore, the Rossby wave component needs to be taken into account when studying wave-convection feedback in the MJO.

In order to include the Rossby wave component, a three-dimensional model needs to be used instead of the two-dimensional model which was often used for the pure Kelvin wave. What are the conditions for the Rossby wave component to be strong in the three-dimensional model? Yamagata (1987) pointed out that the Kelvin-Rossby wave pattern forced by a moving heating source is sensitive to the speed of the heating. The Kelvin component increases montonically with increasing speed, while the Rossby component decreases montonically with increasing speed. Fig. 14a shows the ratio between the maximum pressure of the Rossby component and that of the Kelvin component along the equator. It decreases montonically with increasing speed. The sensitivity is high only when the damping is weak. For example, Fig. 15 shows the wave pattern when the heating moves (a) westward, (b) slowly eastward, and (c) fastly eastward when the damping is weak, and corresponding cases (d, e, f) when the damping is strong. Under weak damping, when the heating moves westward (Fig. 15a), the wave pattern is dominated by the Rossby component. When the heating moves slowly eastward (Fig. 15b), the wave pattern looks similar to the observed pattern. When the heating moves fastly eastward (Fig. 15c), the wave pattern is similar to a pure Kelvin wave. Under strong damping, the wave pattern is not sensitive to the moving speed of the heating (Fig. 15d-f). Therefore the two

conditions for the Rossby wave component to be strong are: (1) weak damping, and (2) slow moving speed of the heating.

One of the key questions that the wave-convection feedback theories are trying to answer is: why does the observed MJO have a slow phase speed? In the Kelvin wave model, this is translated to: why is the slow Kelvin wave preferred than the fast Kelvin wave? From the above results, we know that the observed MJO is not a slow Kelvin wave, but resembles a slow Kelvin-Rossby wave. Therefore, in the Kelvin-Rossby wave model, the question becomes: *why is the slow Kelvin-Rossby wave preferred than the fast Kelvin wave or the wesward-propagating Rossby wave?*

5. Summary

A Kelvin-wave conceptual model has often been used in studying wave-convection feedback in the Madden-Julian Oscillation (MJO). In this study, long term observations from tropical sounding stations and NCEP reanalysis, supplemented by measurements from the Tropical Ocean Global Atmosphere (TOGA) Coupled Ocean Atmosphere Response Experiment, are used to study whether the equatorial wave structure of the MJO is similar to the Kelvin wave. All datasets are filtered using a 30-70 day bandpass filter. The long-term MJO composites are constructed using linear correlation and linear regression with respect to precipitation.

The observed equatorial wave structure of the MJO is different from the Kelvin wave, in that the geopotential height lags the zonal wind by a quarter cycle, which is different from the in-phase relationship in the Kelvin wave.

The horizontal wave structure of the MJO is similar to the Matsuno-Gill pattern with a strong Rossby wave component. Based on the Gill model, the strong Rossby wave component significantly shifts the *equatorial* geopotential height anomaly westward, and makes the equatorial wave structure different from the Kelvin wave.

It is shown that the wave-convection feedback mechanisms in the observed Kelvin-Rossby wave are different from those in the Kelvin wave model. This is because the Rossby wave component significantly shifts the equatorial temperature anomaly westward, and changes its phase relation with the heating terms such as the free troposphere moisture convergence, the boundary layer moisture convergence, the surface heat flux, and the local drying of moisture. Therefore, the Rossby wave component needs to be taken into account when studying wave-convection feedback in the MJO.

REFERENCES

Bergman, J. W., H. H. Hendon, K. M. Weickmann, 2001: Intraseasonal Air-Sea Interactions at the Onset of El Nino. *Journal of Climate*, 14, 1702-1719.

Chao, W. C., 1987: On the origin of the tropical intraseasonal oscillation. *J. Atmos. Sci.*, **44**, 1940-1949; Corrigendum, 45, 1283.

Chen, S. S., R. A. Houze., and B. E. Mapes, 1996: Multiscale variability of deep convection in relation to large-scale circulation in TOGA COARE. *J. Atmos. Sci.*, 53, 1380-1409.

Gill, A. E., 1980: Some simple solutions for heat-induced tropical circulation. *Quart. J. Roy. Meteor. Soc.*, **106**, 447-462

Hayashi, Y., and A. Sumi, 1986: The 30-40 day oscillation simulated in an "aqua planet" model. *J. Meteor. Soc. Japan.*, 64, 451-466.

Hayashi, Y., and D. G. Golder, 1993: Tropical 40-50 and 25-30-day oscillations appearing in realistic and idealized GFDL climate models and the ECMWF dataset. *J. Atmos. Sci.*, 50, 464-494.

Hayashi, Y., and S. Miyahara, 1987: A three-dimensional linear response model of the tropical intraseasonal oscillation. *J. Meteor. Soc. Japan*, 65, 843-857.

Hendon, H. H., and B. Liebmann, 1990: A composite study of onset of the Australia monsoon. *J. Atmos. Sci.*, 47, 2227-2240.

Hendon, H. H., and M. L. Salby, 1994: The life cycle of the Madden-Julian oscillation. *J. Atmos. Sci.*, 51, 2225-2237.

Hendon, H. H., and M. L. Salby, 1996: Planetary-scale interactions forced by intraseasonal variations of observed convection. *J. Atmos. Sci.*, 53, 1751-1758.

Hsu, H.-H., 1996: Global view of the intraseasonal oscillation during northern winter. *J. Climate*, **9**, 2386-2406.

Itoh, H., 1989: The mechanism for the scale selection of tropical intraseasonal oscillations. Part I: Selection of wavenumber 1 and the three-scale structure. *J. Atmos. Sci.*, 46, 1779-1798.

Kessler, W. S., and M. J. McPhaden, and K. M. Weickmann, 1995: Forcing of intraseasonal Kelvin waves in the equatorial Pacific. *J. Geophys. Res.*, 100, 10613-10631.

Kiladis, G. N., and K. M. Weickmann, 1992: Circulation anomalies associated with tropical convection during northern winter. *Mon. Wea. Rev.*, **120**, 1900-1923.

Knutson, T. R., and K. M. Weickmann, 1987: The 30-60 day atmospheric oscillation: Composite life cycles of convection and circulation anomalies. *Mon. Wea. Rev.*, **115**, 1407-1436.

Lau, K.-M., and T. J. Phillips, 1986: Coherent fluctuations of extratropical geopotential height and tropical convection in intraseasonal timescales. *J. Atmos. Sci.*, 43, 1164-1181.

Lau, N. C., I. M. Held, and J. D. Neelin, 1988: The Madden-Julian oscillations in an idealized general circulation model. *J. Atmos. Sci.*, **45**, 3810-3831.

Liebmann, B., H. H. Hendon, and J. D. Glick, 1994: The relationship between t tropical cyclones of the western Pacific and Indian Oceans and the Madden-Julian oscillation. *J. Meteor. Soc. Japan*, 72, 401-411.

Madden, R. A., and P. R. Julian, 1971: Detection of a 40-50 day oscillation in the zonal wind in the tropical Pacific. *J. Atmos. Sci.*, **28**, 702-708.

Madden, R. A., and P. R. Julian, 1972: Description of global-scale circulation cells in the tropics with a 40-50 day period. *J. Atmos. Sci.*, **29**, 1109-1123.

Madden, R. A., and P. R. Julian, 1994: Observations of the 40-50-day oscillation -A review. *Mon. Wea. Rev.*, **122**, 814-837.

Matsuno, T., 1966: Quasi-geostrophic motions in the equatorial area. *J. Meteor. Soc. Japan*, 44, 25-43.

Murakami, M., 1979: Large-scale aspects of deep convective activity over the GATE area. *Mon. Wea. Rev.*, **107**, 994-1013.

Murakami, T., and T. Nakazawa, 1985: Tropical 45 day oscillation during the 1979 Northern Hemisphere summer. *J. Atmos. Sci.*, 42, 1107-1122.

Nishi, N., 1989: Observational study on the 30-60 day variations in the geopotential and temperature fields in the equatorial region. *J. Meteor. Soc. Japan*, **67**, 187-203.

Oort, A. H., and J. J. Yienger, 1996: Observed long-term variability in the Hadley circulation and its connection to ENSO. *J. Climate*, 9, 2751-2767.

Parker, D., 1973: Equatorial Kelvin waves at 100 millibars. *Quart. J. Roy. Meteor. Soc.*, **99**, 116-129.

Rui, H., and B. Wang, 1990: Development characteristics and dynamic structure of tropical intraseasonal convection anomalies. *J. Atmos. Sci.*, **47**, 357-379.

Salby, M. L., and H. H. Hendon, 1994: Intraseasonal behavior of clouds, temperature, and motion in the Tropics. *J. Atmos. Sci.*, **51**, 2207-2224.

Salby, M. L., R. B. Garcia, and H. H. Hendon, 1994: Planetary-scale circulations in the presence of climatological and wave-induced heating. *J. Atmos. Sci.*, **51**, 2344-2367.

Sardeshmukh, P. D., M. Newman, and C. R. Winkler, 1999: Dynamically consistent estimates of diabatic heating. Proceedings, 24th Climate Diagnostics and Prediction Workshop, Tucson, AZ, 172-175.

Spencer, R. W., J. R. Christy, and N. C. Grody, 1990: Global atmospheric temperature monitoring with satellite microwave measurements: Method and results 1979-84. *J. Climate*, **3**, 1111-1128.

Takayabu, Y .N., Toshio Iguchi, Misako Kachi, Akira Shibata and Hiroshi Kanzawa, 1999: Abrupt termination of the 1997-98 El Nino in response to a Madden-Julian oscillation. *Nature*, 402, 279-282.

Wang, W., and M. E. Schlesinger, 1999: The dependence on convection parameterization of the tropical intraseasonal oscillation simulated by the 11-layer UIUC atmospheric GCM. *J. Climate*, **12**, 1423-1457.

Weickmann, K. M., G. R. Lussky, and J. E. Kutzbach, 1985: Intraseasonal (30-60 day) fluctuations of outgoing longwave radiation and 250 mb streamfunction during northern winter. *Mon. Wea. Rev.*, 113, 941-961.

Wheeler, M., and G. N. Kiladis, 1999: Convectively coupled equatorial waves: Analysis of clouds and temperature in the wavenumber-frequency domain. *J. Atmos. Sci.*, **56**, 374-399.

Xie, P., and P. A. Arkin, 1997: Global precipitation: A 17-year monthly analysis based on gauge observations, satellite estimates, and numerical model outputs. *Bull. Amer. Meteor. Soc.*, **78**, 2539-2558.

Yamagata, T., 1987. A simple moist model relevant to the origin of intraseasonal distur-

bances in the tropics. *J. Meteor. Soc. Japan*, **65**, 153-165.

Yanai, M., B. Chen, and W.-W. Tung, 2000: The Madden-Julian oscillation observed during the TOGA COARE IOP: Global view. *J. Atmos. Sci., 57*, 2374-2396.

Yasunari, T., 1979: Cloudiness fluctuations associated with the northern hemisphere summer monsoon. *J. Meteor. Soc. Japan*, 57, 227-242.

Zhang, M. H., and M. A. Geller, 1994: Selective excitation of tropical atmospheric waves in wave-CISK: The effect of vertical wind shear. *J. Atmos. Sci.*, **51**, 353-368.

Zhang, M. H., and J. L. Lin, 1997: Constrained variational analysis of sounding data based on column-integrated budgets of mass, heat, moisture, and momentum: Approach and application to ARM measurements. *J. Atmos. Sci.*, **54**, 1503-1524.

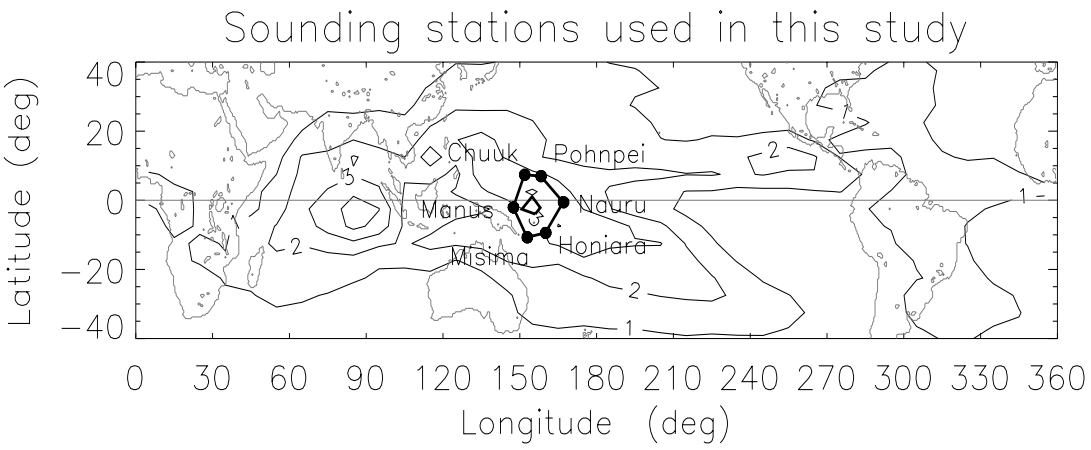
Sounding stations used in this study
Latitude (deg)
40
20
0
−20
−40
0
30
60
90
120
150
180
210
240
270
300
330
360
Longitude (deg)
Chuuk
Pohnpei
Manus
Nauru
Honiara
Misima
1
2
3
4
5

Figure 1:

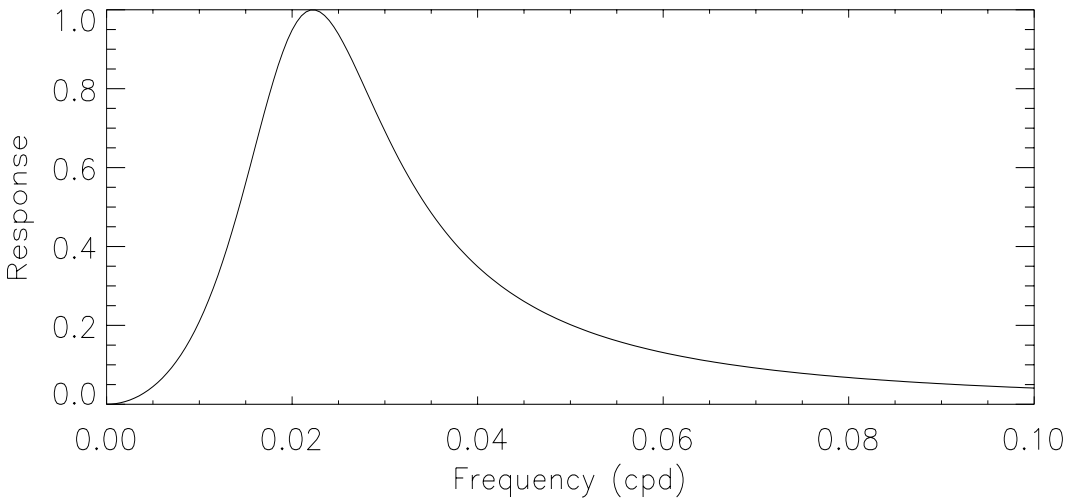
1.0
0.8
0.6
0.4
0.2
0.0
Response
0.00
0.02
0.04
0.06
0.08
0.10
Frequency (cpd)

Figure 2:

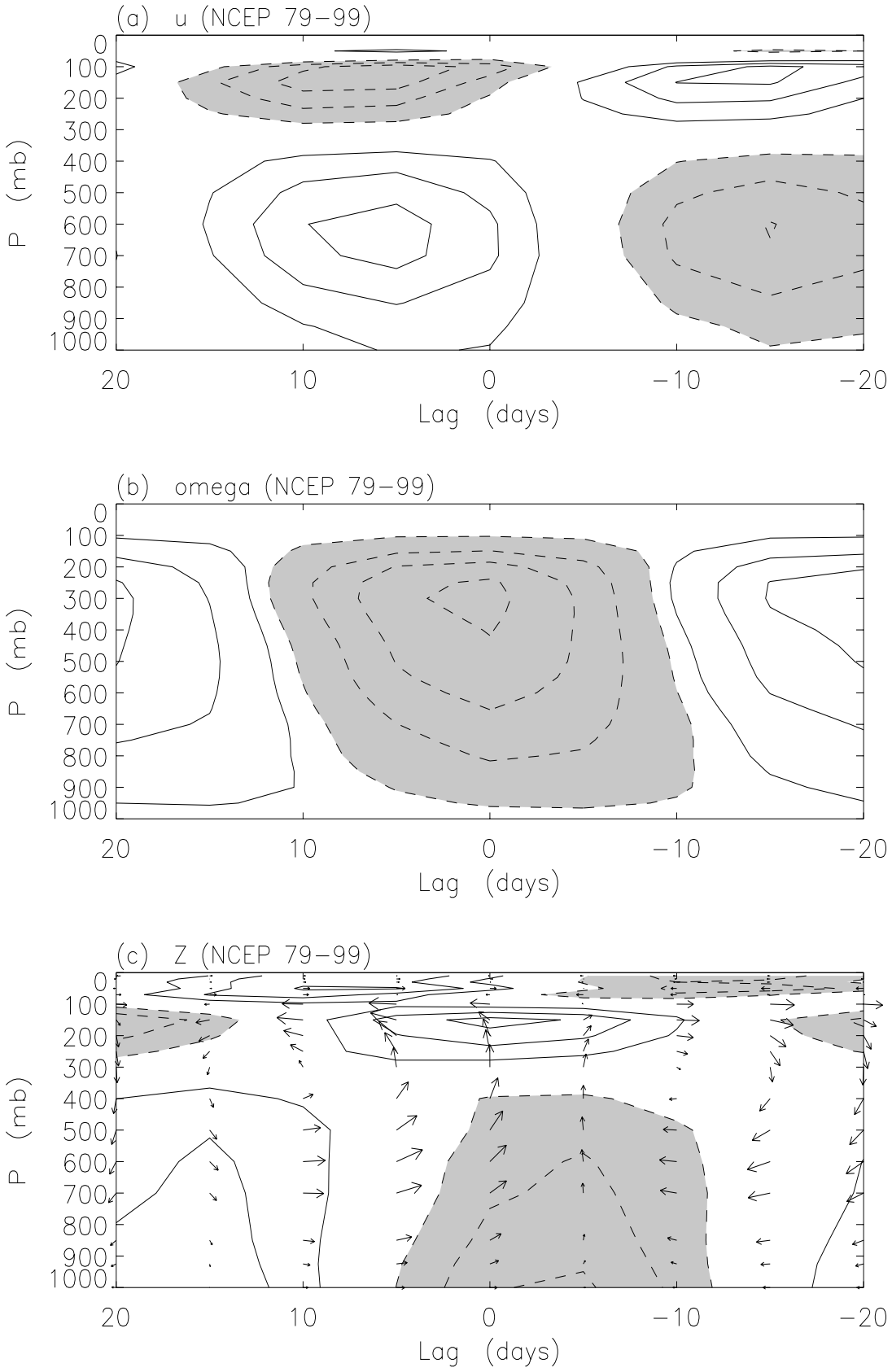
(a) u (NCEP 79−99)
P (mb)
0
100
200
300
400
500
600
700
800
900
1000
20
10
0
−10
−20
Lag (days)
(b) omega (NCEP 79−99)
P (mb)
0
100
200
300
400
500
600
700
800
900
1000
20
10
0
−10
−20
Lag (days)
(c) Z (NCEP 79−99)
P (mb)
0
100
200
300
400
500
600
700
800
900
1000
20
10
0
−10
−20
Lag (days)

Figure 3:

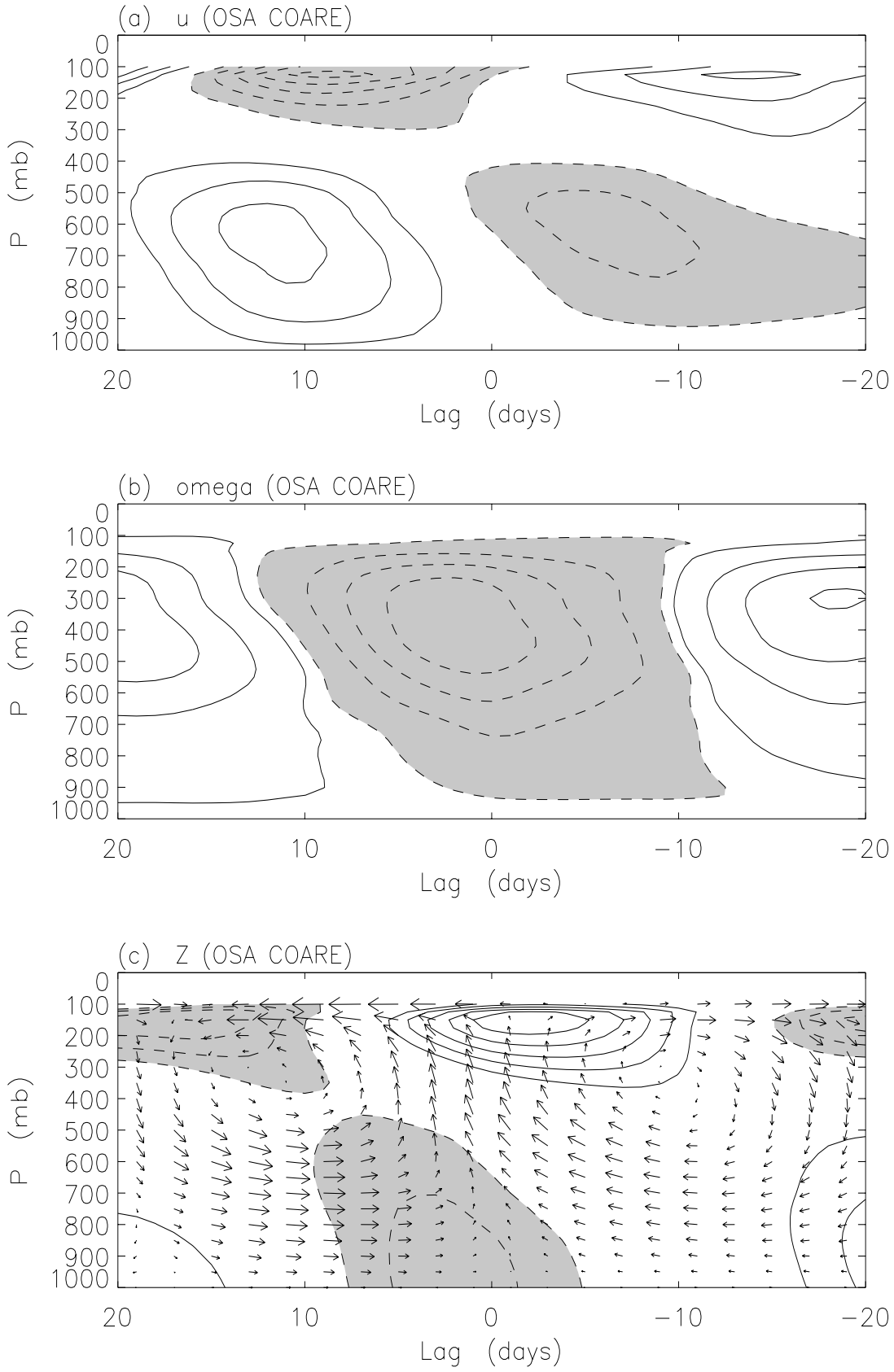
(a) u (OSA COARE)
P (mb)
0
100
200
300
400
500
600
700
800
900
1000
20
10
0
−10
−20
Lag (days)
(b) omega (OSA COARE)
P (mb)
0
100
200
300
400
500
600
700
800
900
1000
20
10
0
−10
−20
Lag (days)
(c) Z (OSA COARE)
P (mb)
0
100
200
300
400
500
600
700
800
900
1000
20
10
0
−10
−20
Lag (days)

Figure 4:

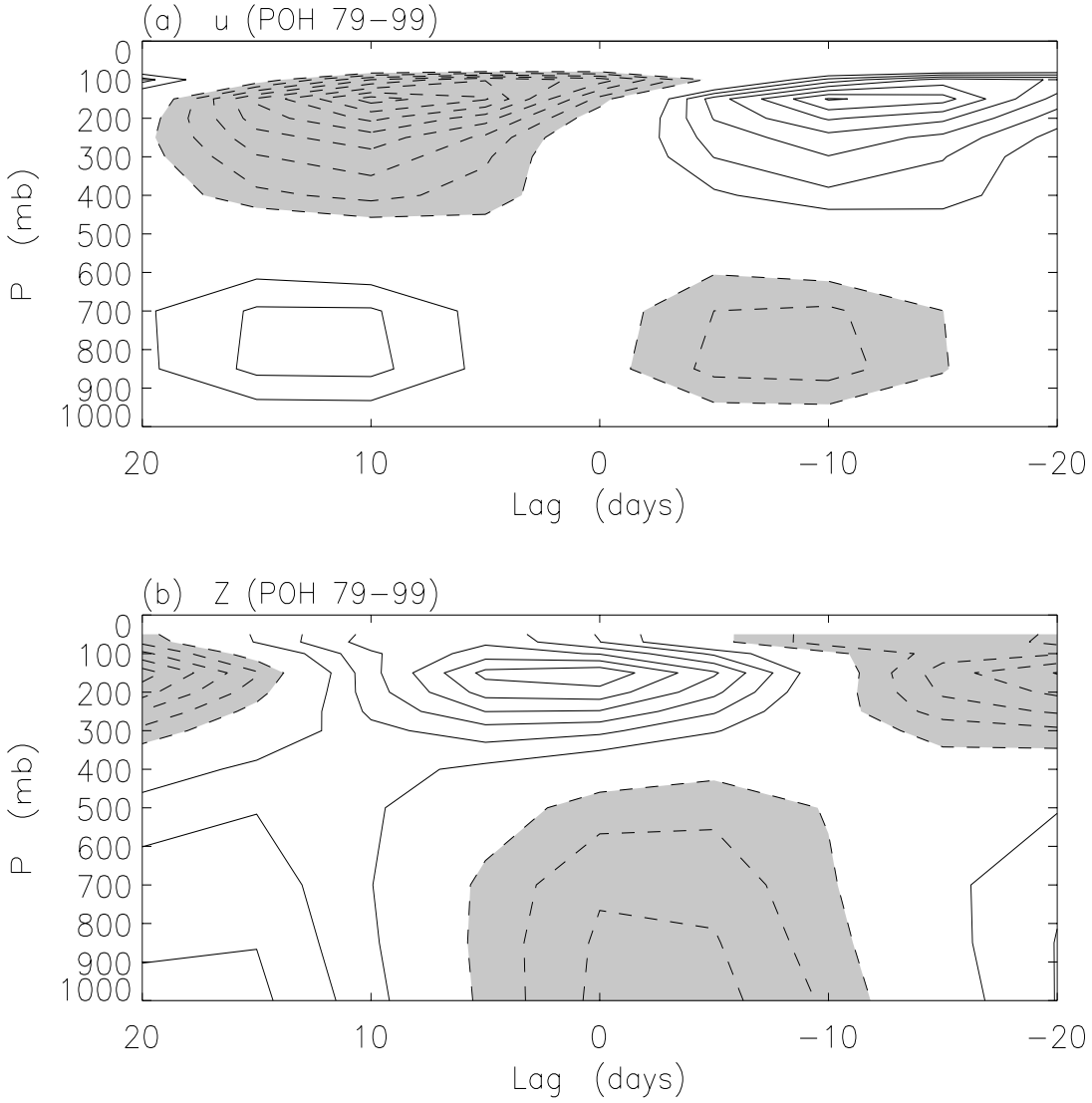
(a) u (POH 79−99)
P (mb)
0
100
200
300
400
500
600
700
800
900
1000
20
10
0
−10
−20
Lag (days)
(b) Z (POH 79−99)
P (mb)
0
100
200
300
400
500
600
700
800
900
1000
20
10
0
−10
−20
Lag (days)

Figure 5:

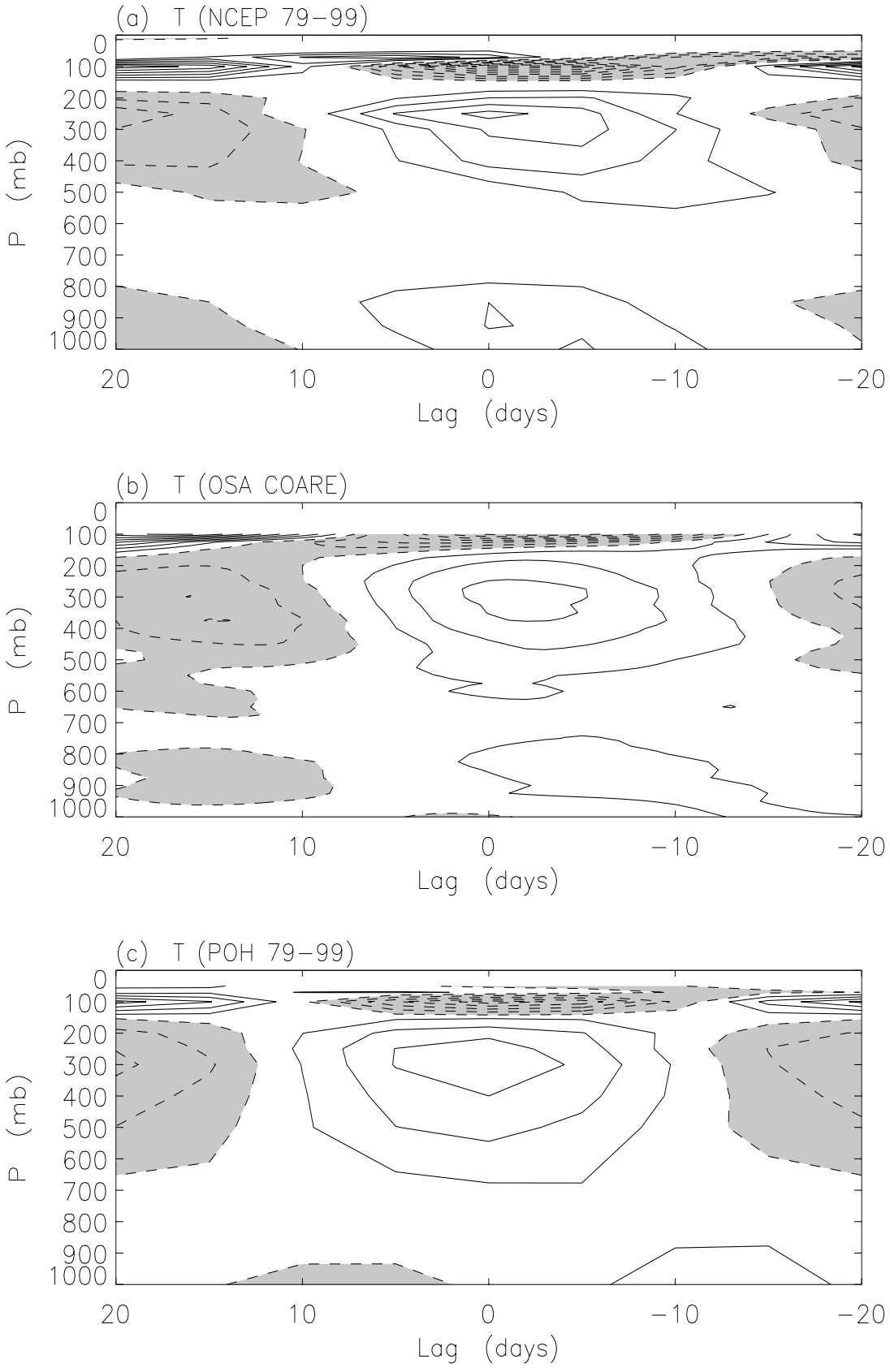
(a) T (NCEP 79−99)
(b) T (OSA COARE)
(c) T (POH 79−99)
P (mb)
0
100
200
300
400
500
600
700
800
900
1000
20
10
0
−10
−20
Lag (days)

Figure 6:

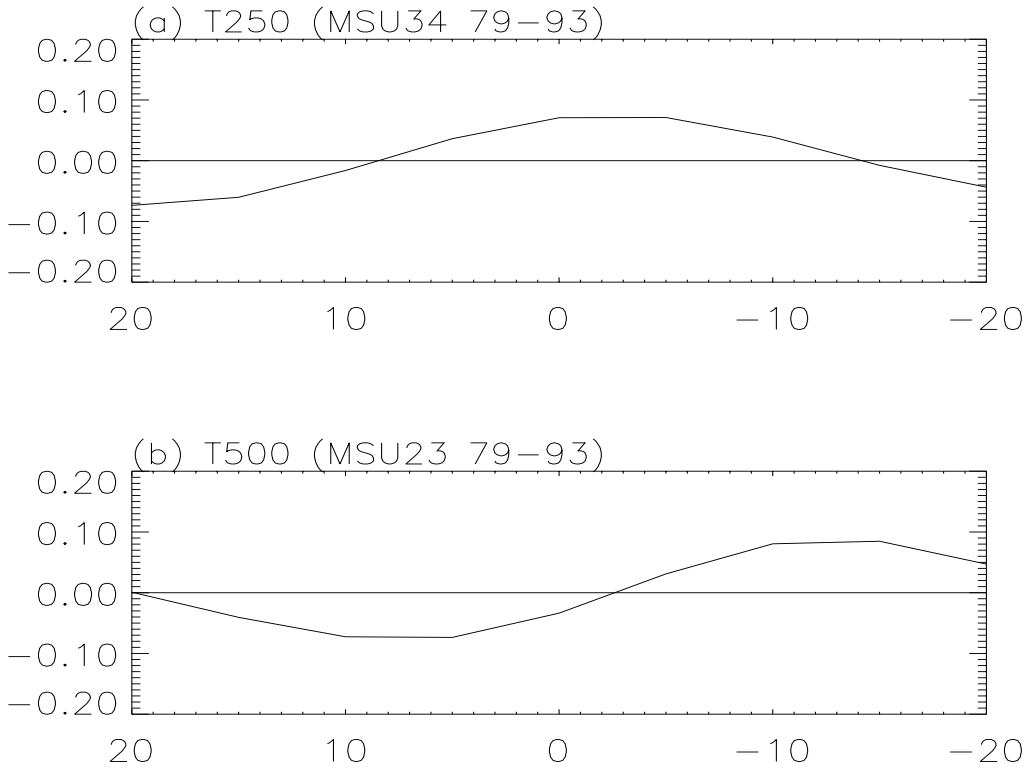
(a) T250 (MSU34 79−93)
0.20
0.10
0.00
−0.10
−0.20
20
10
0
−10
−20
(b) T500 (MSU23 79−93)
0.20
0.10
0.00
−0.10
−0.20
20
10
0
−10
−20

Figure 7:

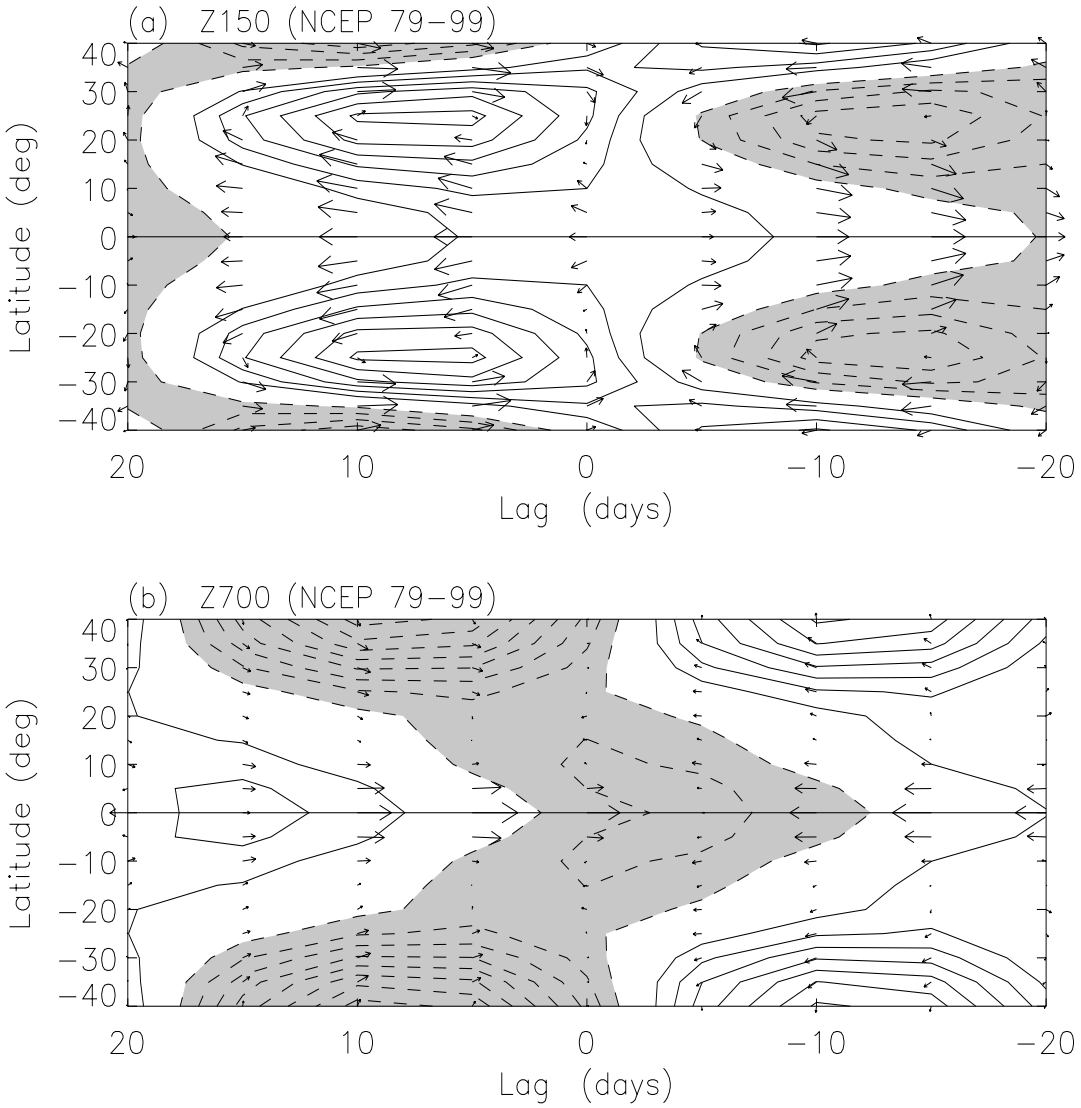
(a) Z150 (NCEP 79−99)
Latitude (deg)
40
30
20
10
0
−10
−20
−30
−40
20
10
0
−10
−20
Lag (days)
(b) Z700 (NCEP 79−99)
Latitude (deg)
40
30
20
10
0
−10
−20
−30
−40
20
10
0
−10
−20
Lag (days)

Figure 8:

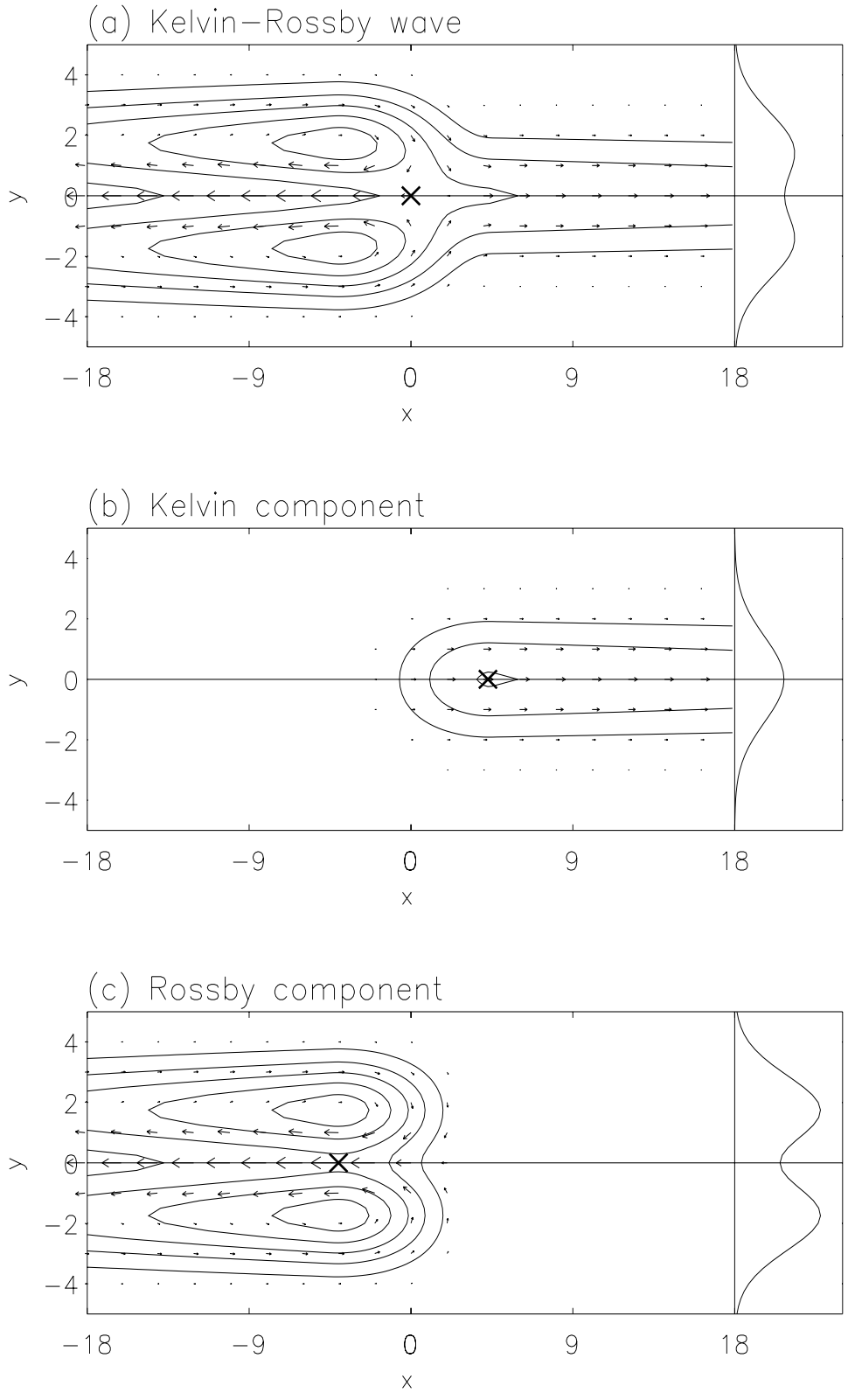
(a) Kelvin−Rossby wave
(b) Kelvin component
(c) Rossby component
y
x
4
2
0
−2
−4
−18
−9
0
9
18

Figure 9:

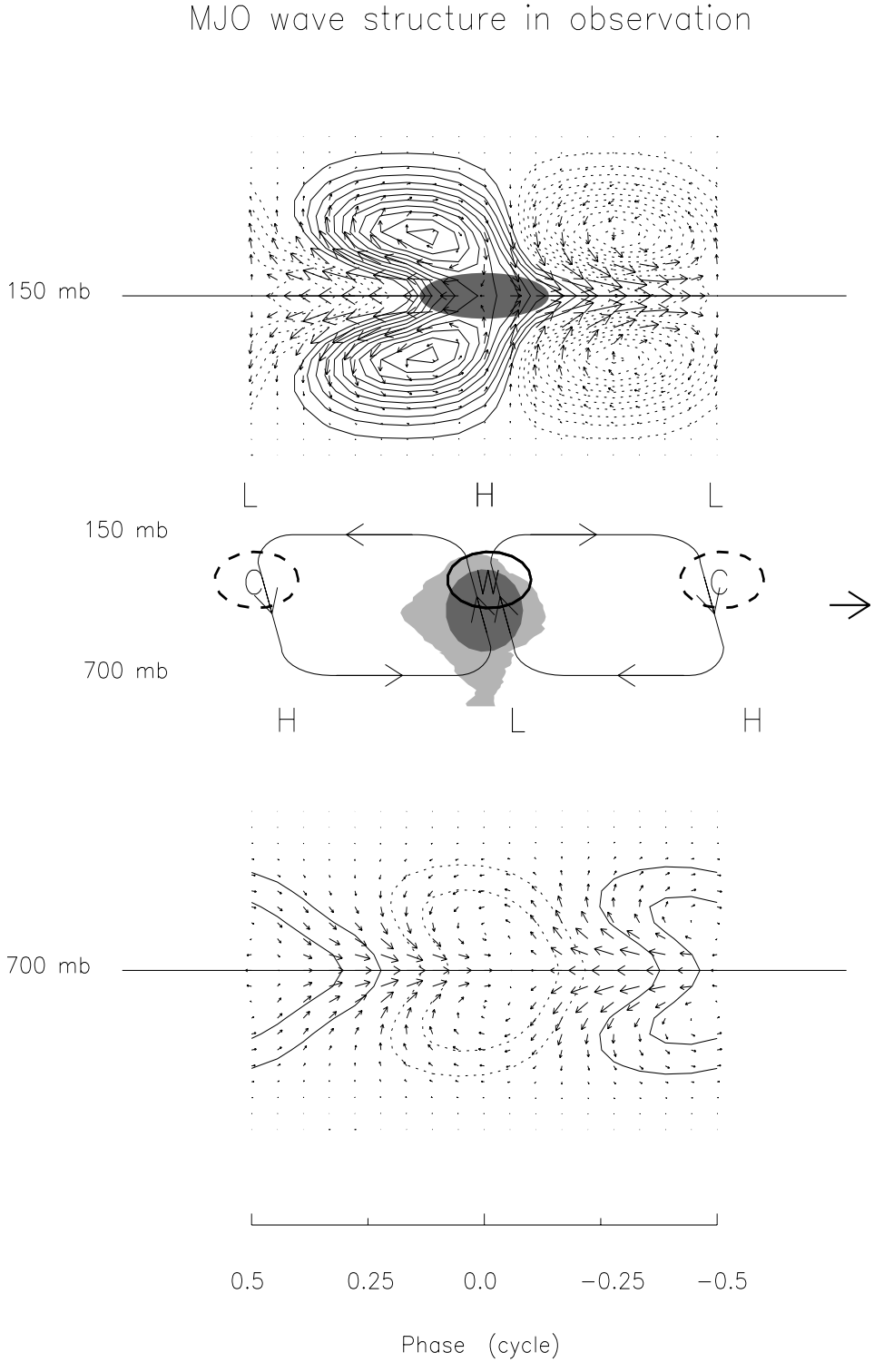
MJO wave structure in observation
150 mb
L
H
L
150 mb
C
W
C
700 mb
H
L
H
700 mb
0.5
0.25
0.0
−0.25
−0.5
Phase (cycle)

Figure 10:

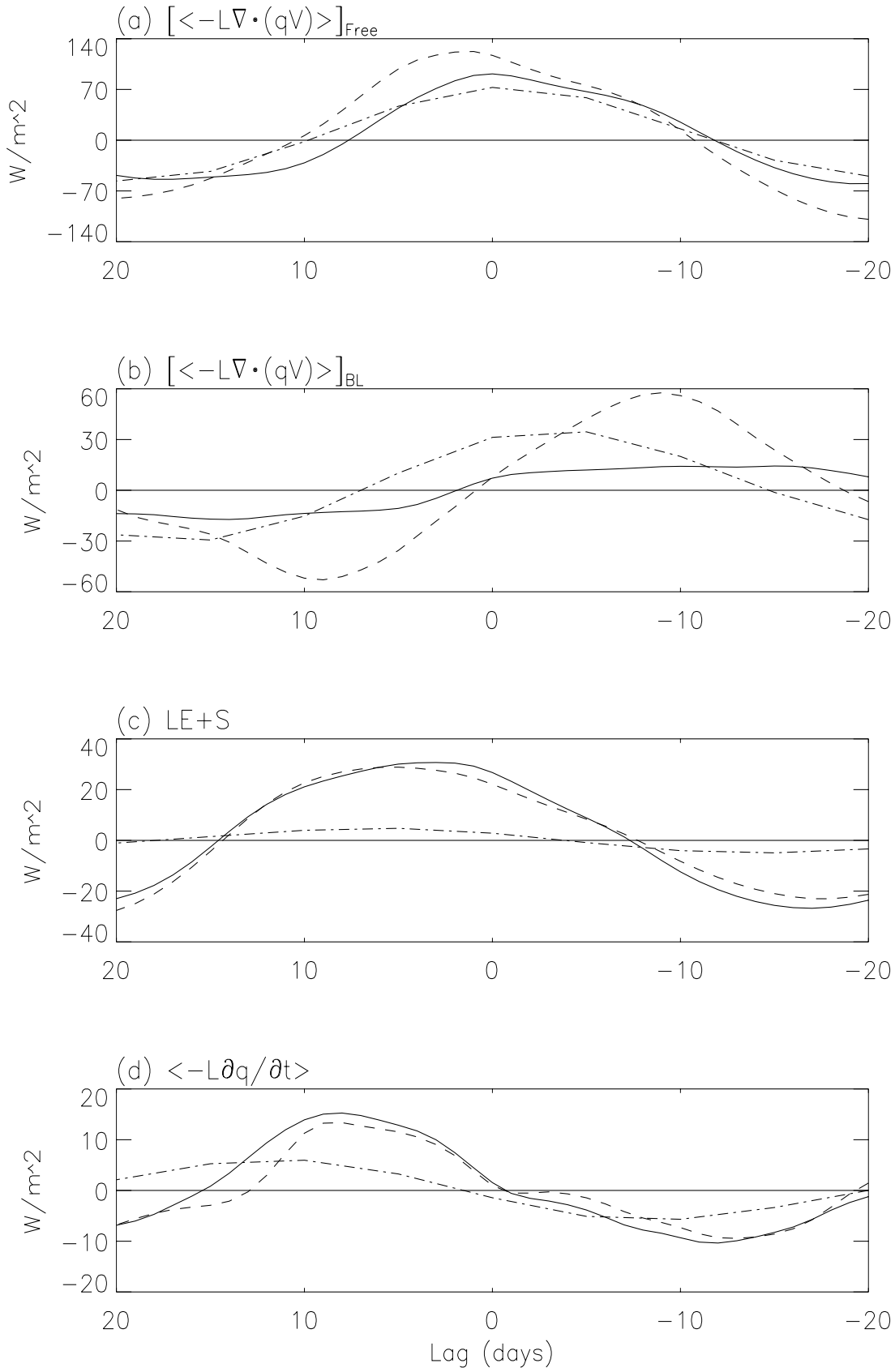
(a) [<−L∇•(qV)>]Free
140
70
0
−70
−140
W/m^2
20
10
0
−10
−20
(b) [<−L∇•(qV)>]BL
60
30
0
−30
−60
W/m^2
20
10
0
−10
−20
(c) LE+S
40
20
0
−20
−40
W/m^2
20
10
0
−10
−20
(d) <−L∂q/∂t>
20
10
0
−10
−20
W/m^2
20
10
0
−10
−20
Lag (days)

Figure 11:

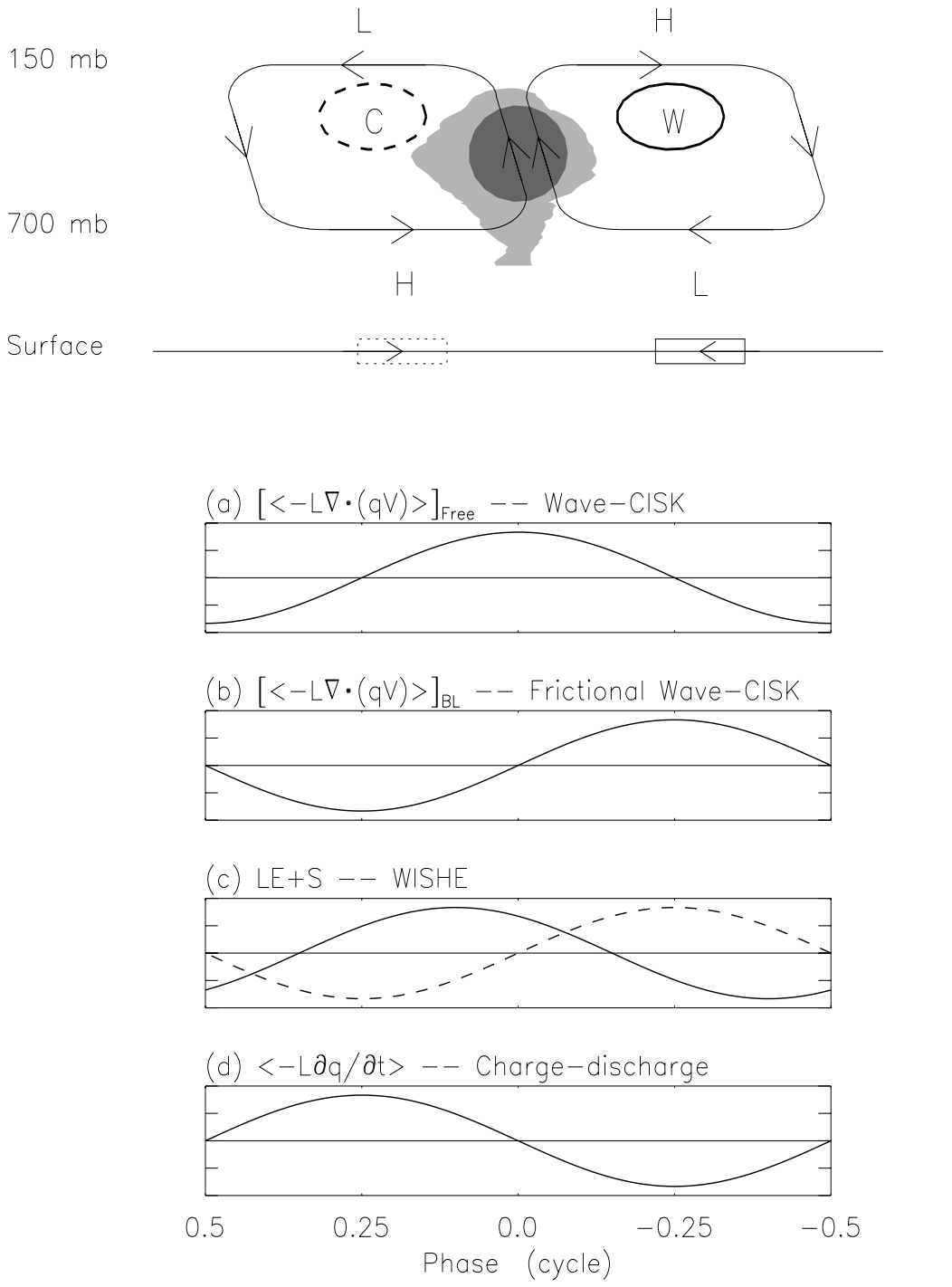
Wave−convection feedback in theoretical Kelvin wave
L
H
150 mb
C
W
700 mb
H
L
Surface
(a) [<−L∇•(qV)>]Free −− Wave−CISK
(b) [<−L∇•(qV)>]BL −− Frictional Wave−CISK
(c) LE+S −− WISHE
(d) <−L∂q/∂t> −− Charge−discharge
0.5
0.25
0.0
−0.25
−0.5
Phase (cycle)

Figure 12:

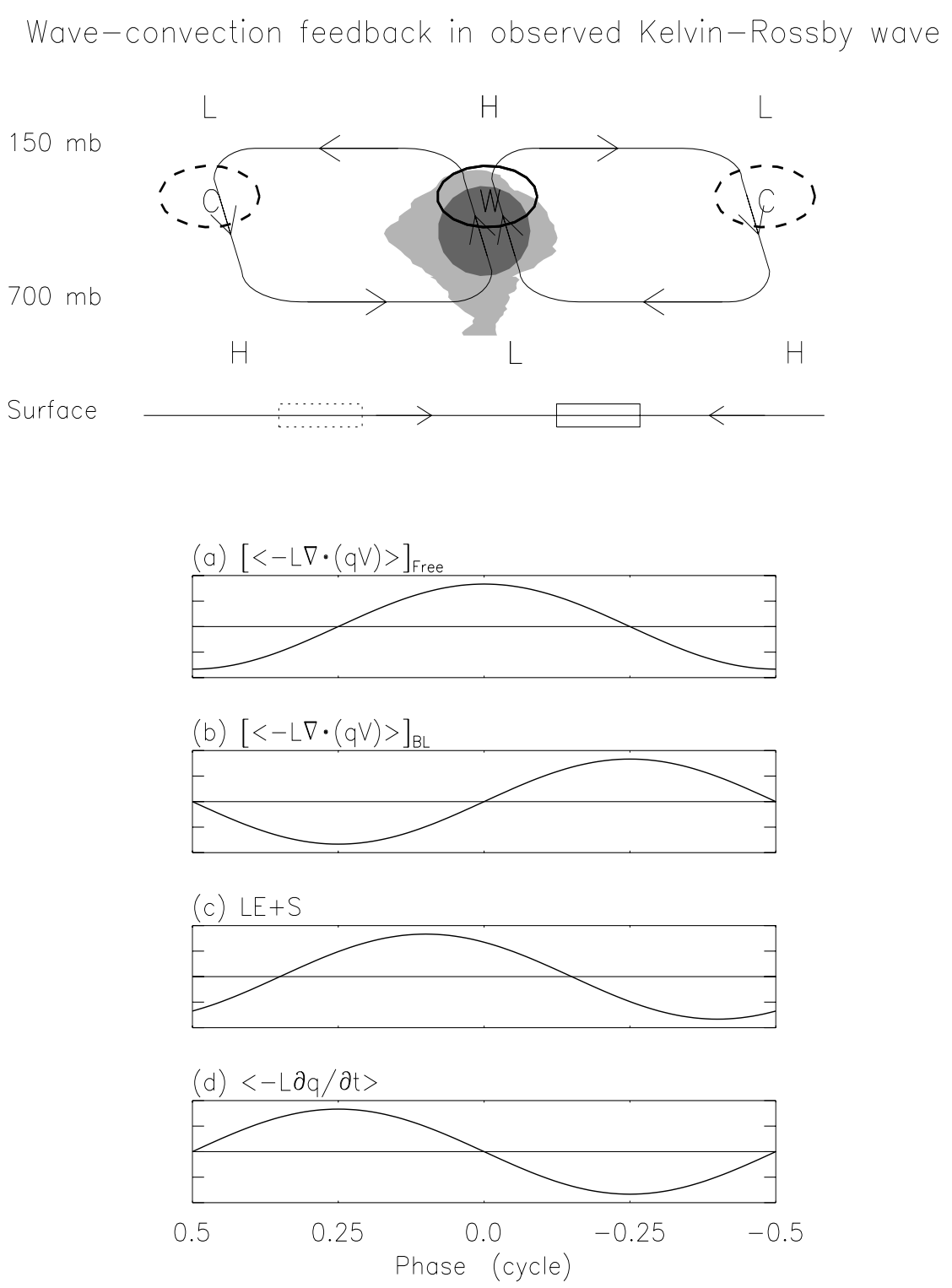
Wave−convection feedback in observed Kelvin−Rossby wave
L
H
L
150 mb
C
W
C
700 mb
H
L
H
Surface
(a) [<−L∇•(qV)>]Free
(b) [<−L∇•(qV)>]BL
(c) LE+S
(d) <−L∂q/∂t>
0.5
0.25
0.0
−0.25
−0.5
Phase (cycle)

Figure 13:

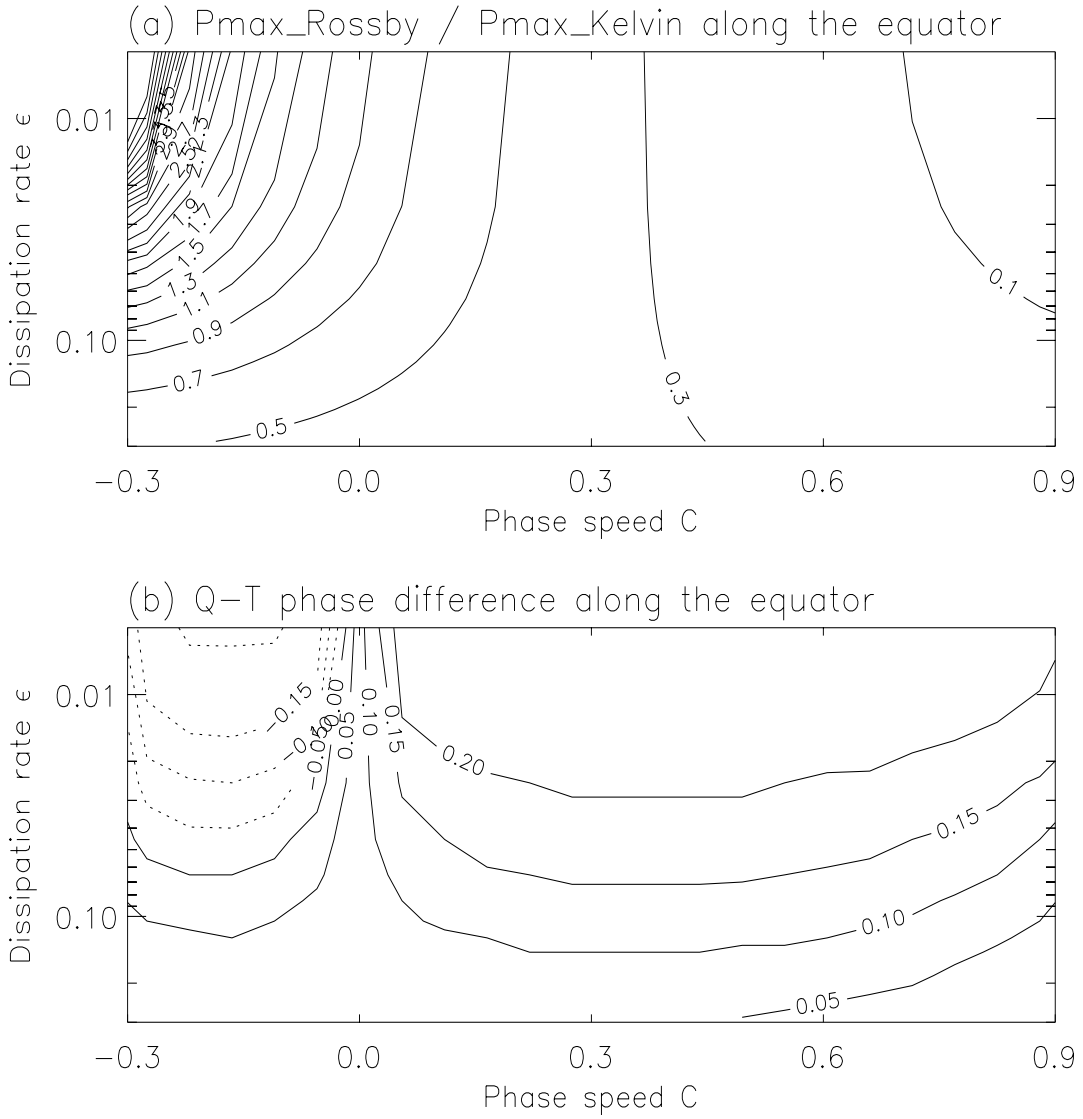
(a) Pmax_Rossby / Pmax_Kelvin along the equator
Dissipation rate ϵ
0.01
0.10
−0.3
0.0
0.3
0.6
0.9
Phase speed C
0.1
0.3
0.5
0.7
0.9
1.1
1.3
1.5
1.7
1.9
2.1
2.3
2.5
(b) Q−T phase difference along the equator
Dissipation rate ϵ
0.01
0.10
−0.3
0.0
0.3
0.6
0.9
Phase speed C
0.20
0.15
0.10
0.05
0.00
−0.05
−0.10
−0.15

Figure 14:

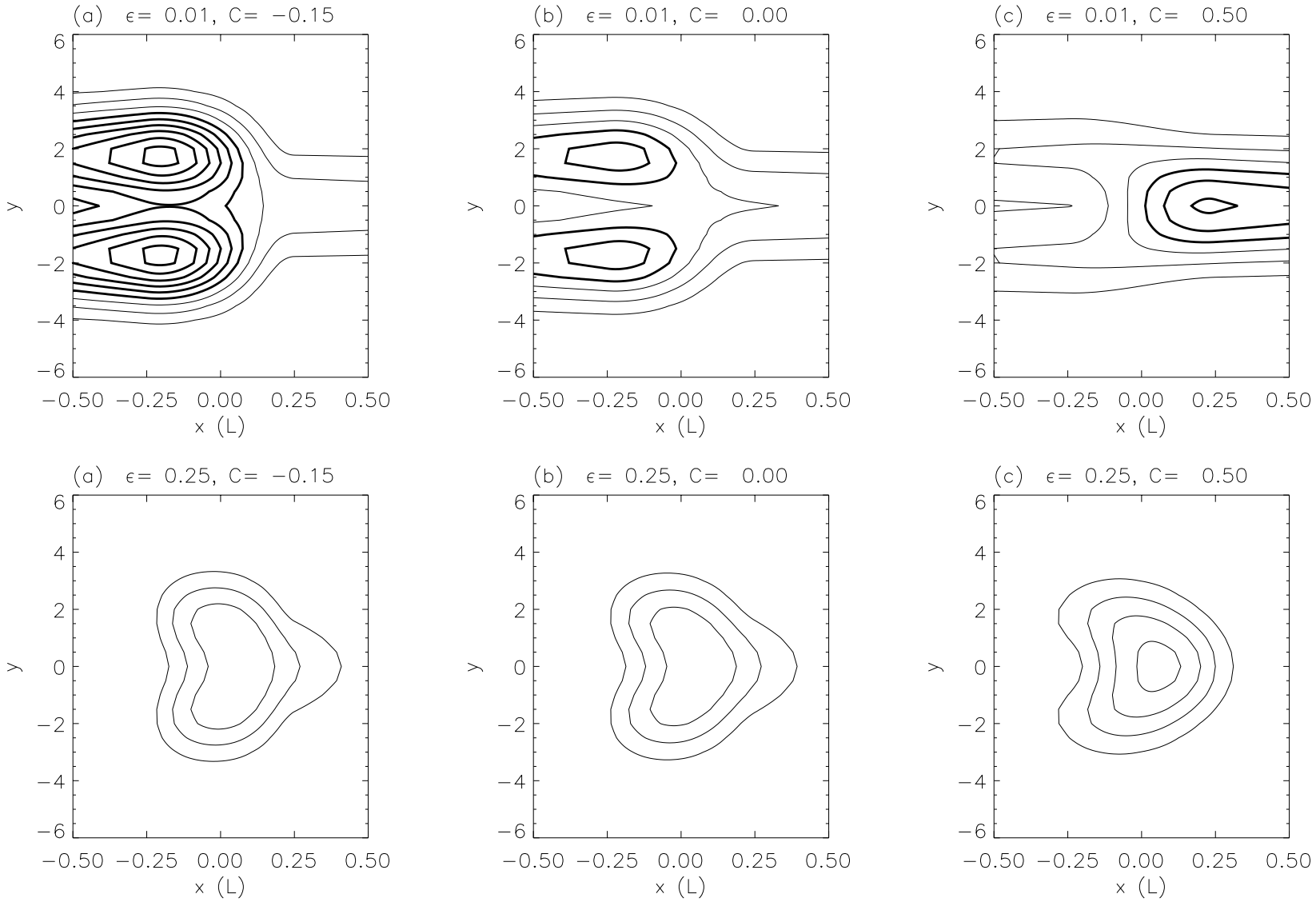
(a) ϵ= 0.01, C= −0.15
(b) ϵ= 0.01, C= 0.00
(c) ϵ= 0.01, C= 0.50
(a) ϵ= 0.25, C= −0.15
(b) ϵ= 0.25, C= 0.00
(c) ϵ= 0.25, C= 0.50
y
x (L)
6
4
2
0
−2
−4
−6
−0.50 −0.25 0.00 0.25 0.50

Figure 15: